

# A guide to the reconstruction of the autopodia of Tetrapoda through 3D technology: the case of *Neuquensaurus australis* (Sauropoda: Titanosauria)

AGUSTÍN ROBERTO RUELLA<sup>1</sup>  
AGUSTÍN PÉREZ MORENO<sup>2,3</sup>  
YANINA HERRERA<sup>2,3</sup>

1. División Paleontología Vertebrados, Museo de La Plata, Facultad de Ciencias Naturales y Museo, Universidad Nacional de La Plata. Paseo del Bosque s/n, B1900FWA La Plata, Buenos Aires, Argentina.
2. División Paleontología Vertebrados, Edificio Anexo Laboratorios I y II, Museo de La Plata, Facultad de Ciencias Naturales y Museo, Universidad Nacional de La Plata. Avenida 122 y 60, B1900 La Plata, Buenos Aires, Argentina.
3. Consejo Nacional de Investigaciones Científicas y Técnicas (CONICET). Godoy Cruz 2290, C1425FQB Ciudad Autónoma de Buenos Aires, Argentina.

Recibido: 17 de agosto 2023 - Aceptado: 4 de octubre 2023 - Publicado: 6 de marzo 2024

**Para citar este artículo:** Agustín Roberto Ruella, Agustín Pérez Moreno, & Yanina Herrera. (2024). A guide to the reconstruction of the autopodia of Tetrapoda through 3D technology: the case of *Neuquensaurus australis* (Sauropoda: Titanosauria). *Publicación Electrónica de la Asociación Paleontológica Argentina* 24(1): 26–43.

**Link a este artículo:** <http://dx.doi.org/10.5710/PEAPA.04.10.2023.483>

©2024 Ruella, Pérez Moreno, & Herrera



This work is licensed under

**CC BY-NC 4.0**



ISSN 2469-0228

Asociación Paleontológica Argentina  
Maipú 645 1° piso, C1006ACG, Buenos Aires  
República Argentina  
Tel/Fax (54-11) 4326-7563  
Web: [www.apaleontologica.org.ar](http://www.apaleontologica.org.ar)

# A GUIDE TO THE RECONSTRUCTION OF THE AUTOPODIA OF TETRAPODA THROUGH 3D TECHNOLOGY: THE CASE OF *NEUQUENSAURUS AUSTRALIS* (SAUROPODA: TITANOSAURIA)

AGUSTÍN ROBERTO RUELLA<sup>1</sup>, AGUSTÍN PÉREZ MORENO<sup>2,3</sup>, AND YANINA HERRERA<sup>2,3</sup>

<sup>1</sup>División Paleontología Vertebrados, Museo de La Plata, Facultad de Ciencias Naturales y Museo, Universidad Nacional de La Plata. Paseo del Bosque s/n, B1900FWA La Plata, Buenos Aires, Argentina. [agustinruella@gmail.com](mailto:agustinruella@gmail.com)

<sup>2</sup>División Paleontología Vertebrados, Edificio Anexo Laboratorios I y II, Museo de La Plata, Facultad de Ciencias Naturales y Museo, Universidad Nacional de La Plata. Avenida 122 y 60, B1900 La Plata, Buenos Aires, Argentina. [aperezmoreno7@gmail.com](mailto:aperezmoreno7@gmail.com); [yaninah@fcnym.unlp.edu.ar](mailto:yaninah@fcnym.unlp.edu.ar)

<sup>3</sup>Consejo Nacional de Investigaciones Científicas y Técnicas (CONICET). Godoy Cruz 2290, C1425FQB Ciudad Autónoma de Buenos Aires, Argentina.

 ARR: <https://orcid.org/0009-0002-9389-9352>; APM: <https://orcid.org/0000-0003-0674-2585>; YH: <https://orcid.org/0000-0002-2020-1227>

**Abstract.** This contribution presents a detailed methodology for reconstructing the anterior and posterior autopodia (manus and pes elements) of the sauropod dinosaur *Neuquensaurus australis*. The study utilizes various techniques, including digital three-dimensional (3D) scanning, reconstruction, retrodeformation, scaling, texturing, rendering, 3D printing, and mounting, to create accurate representations of the fossil elements. Two different scanning devices were employed to capture high-resolution 3D models of the fossil elements. The scanned data was processed to align and fuse the points, resulting in detailed 3D models. Related taxa such as *Argyrosaurus superbus* and 3D modeling techniques were used to reconstruct missing elements. Scaling calculations were performed based on comparative analysis with other titanosaurs to estimate the size of the missing elements. Retrodeformation was applied to correct taphonomic distortion and restore the original shape of the fossil elements. Texturing and rendering techniques were also employed to enhance the visual quality of the 3D models. The 3D models were subsequently 3D printed using white polylactic acid (PLA) filament. Creating physical replicas is useful for further studies, educational purposes, and public outreach. We highlight the advantages of 3D printing in paleontology, such as cost-effectiveness and accessibility, as it creates accurate replicas without compromising the original fossils. Overall, the presented methodologies demonstrate the potential of 3D technologies in paleontological research. The combination of scanning, reconstruction, retrodeformation, scaling, texturing, rendering, and 3D printing provides a comprehensive approach to accurately reconstructing and visualizing fossil elements. These techniques contribute to a better understanding of extinct vertebrates and their biomechanics.

**Key words.** Scanner. 3D model. Retrodeformation. Museo de La Plata. 3D printing. Dinosauria.

**Resumen.** GUÍA PARA LA RECONSTRUCCIÓN DE LOS AUTOPODIOS DE LOS TETRAPODA MEDIANTE TECNOLOGÍA 3D: EL CASO DE *NEUQUENSAURUS AUSTRALIS* (SAUROPODA: TITANOSAURIA). Esta contribución presenta una metodología detallada para la reconstrucción de los autopodios anteriores y posteriores (elementos de la mano y el pie) del dinosaurio saurópodo *Neuquensaurus australis*. El estudio utiliza varias técnicas, como el escaneado digital tridimensional (3D), la reconstrucción, la retrodeformación, el escalado, la texturización, la renderización, la impresión 3D y el montaje, para crear representaciones precisas de los elementos fósiles. Se emplearon dos dispositivos de escaneado diferentes para capturar modelos 3D de alta resolución de los elementos fósiles. Los datos escaneados se procesaron para alinear y fusionar los puntos, con lo que se obtuvieron modelos 3D detallados. Taxones relacionados, como *Argyrosaurus superbus* y técnicas de modelado 3D fueron usados para la reconstrucción de los elementos faltantes. Se realizaron cálculos de escala basados en análisis comparativos con otros titanosaurios para estimar el tamaño de los elementos faltantes. Se aplicó la retrodeformación para corregir la distorsión tafonómica y restaurar la forma original de los elementos fósiles. También se emplearon técnicas de texturizado y renderizado para mejorar la calidad visual de los modelos 3D. Los modelos 3D se imprimieron posteriormente en 3D usando filamento ácido poliláctico (PLA) blanco. La creación de réplicas físicas es útil para estudios posteriores, fines educativos y divulgación pública. Destacamos las ventajas de la impresión 3D en paleontología, como la rentabilidad y la accesibilidad, ya que crea réplicas precisas sin poner en peligro los fósiles originales. En conjunto, las metodologías presentadas demuestran el potencial de las tecnologías 3D en la investigación paleontológica. La combinación de escaneado, reconstrucción, retrodeformación, escalado, texturizado, renderizado e impresión 3D proporciona un enfoque integral para reconstruir y visualizar con precisión elementos fósiles. Estas técnicas contribuyen a una mejor comprensión de los vertebrados extintos y su biomecánica.

**Palabras clave.** Escáner. Modelo 3D. Retrodeformación. Museo de La Plata. Impresión 3D. Dinosauria.

THE HISTORY of assembling skeletal mounts for extinct vertebrates is rich and captivating. It all began in 1789 when

the first fossil skeletal mount was created for *Megatherium americanum* Cuvier, 1796, drawing from Juan Bautista Bru's

studies. However, dinosaur skeletal mounts took nearly a century to gain popularity.

A pivotal moment in this field occurred in the early 1900s when Andrew Carnegie played a significant role in distributing skeletal mounts and casts of *Diplodocus carnegii* Hatcher, 1901 (Fig. 1). This distribution included a substantial portion of known skeletal elements from the same dinosaur species, making it a remarkable milestone in paleontological research (Otero & Gasparini, 2014).

Dinosaur skeletal mounts hold paramount importance in certain research areas, particularly biomechanics. Precise knowledge of skeletal proportions and their spatial arrangement is crucial for studies on locomotion, body weight, feeding strategies, and functional morphology (Stevens & Parrish, 1999; Hutchinson & Garcia, 2002; Hutchinson *et al.*, 2005; Xing *et al.*, 2009; Mallison, 2010a, 2010b, 2011; Stevens, 2013; Reiss & Mallison, 2014);

however, these fossil skeletons are rarely found complete.

Sauropods particularly have a great preservational bias against their bones due to their large sizes, fragility, and pneumatization (Wedel, 2003a, 2003b). Most sauropod skeletal mounts are composed of either multiple specimens or incorporate some sculpted elements based upon real fossils or closely related species. Traditionally, overlapping specimens of similar sizes (Hatcher, 1901) or scaled-up or down specimens of different sizes (Janensch, 1950) were used to create the mounts. However, many taxa are known from multi-specimen bonebeds with a large size disparity. Thus, the skeletal proportions of such taxa have been known only through rigorous skeletal drawings (Paul & Chase, 1989).

In recent years, virtual paleontology has made tremendous strides. According to Sutton *et al.* (2014), virtual paleontology involves studying fossils through interactive

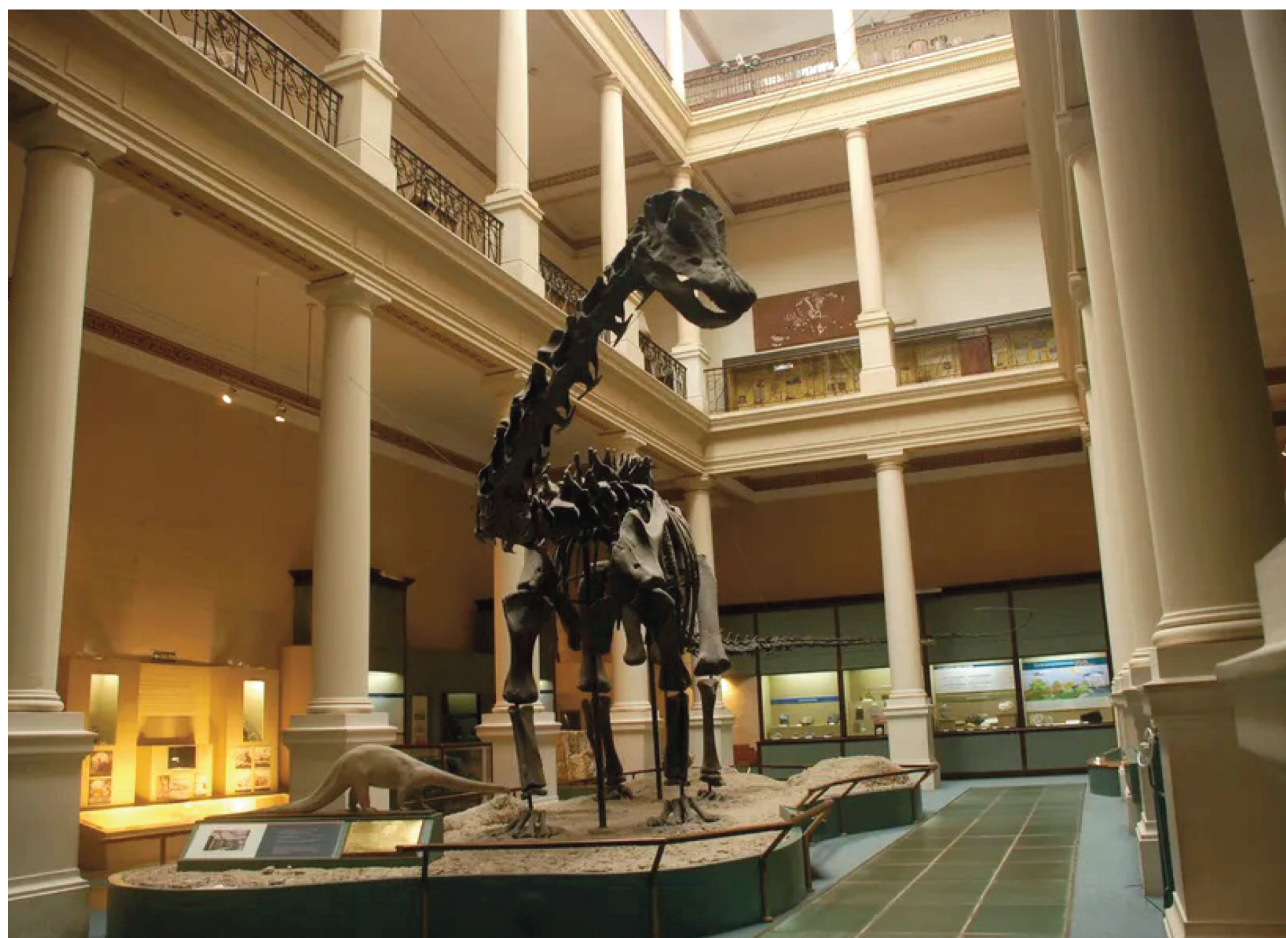


Figure 1. *Diplodocus carnegii* cast mount at the Museo de La Plata, Argentina.

digital visualizations, known as virtual fossils. This cutting-edge approach utilizes advanced imaging and computer technologies, such as computer-aided scanning, digitization techniques, digital visualization, and computational analyses (Lautenschlager, 2016).

As highlighted by Mallison & Wings (2014), three-dimensional (3D) digital models of fossils offer various advantages. They enable the archiving, analysis, and visualization of specimens that may be difficult or impossible to access physically while safeguarding delicate specimens from potential damage through handling (Vidal & Díez Díaz, 2017). This innovative technique revolutionizes how researchers and enthusiasts can explore and understand prehistoric life, opening up new possibilities for scientific discoveries and education. With virtual paleontology, numerous research areas can overcome many of the disadvantages of physical isolation methods and benefit from the use of 3D digitization of specimens, like in geometric morphometric and finite element analyses (Arbour & Currie, 2012), virtual dissection and sectioning (Klinkhamer *et al.*, 2017), ichnology (Breithaupt *et al.*, 2003), and biomechanics (Mallison, 2010a). The case of *Neuquensaurus australis* (Lydekker, 1893) is an excellent example to apply this cutting-edge approach for three main reasons: 1) the amount of overlapping autopodial elements; 2) the damage inherent to the elements assigned to this taxon and; 3) the deterioration that the specimen has suffered over time in the exhibition at the Museo de La Plata (MLP).

Since its mounting at the beginning of the 20th century, the specimen of *Neuquensaurus* exhibited in the MLP has been relocated several times within the same museum (Fig. 2). As a consequence of the rearrangement of the museum's pieces, two problems occurred: 1) it has been reassembled with anatomical errors and 2) it has lost pieces, mainly from the tail and feet, with the passage of time. Given this situation, the authorities of the MLP and the Manager of the División Paleontología Vertebrados established to restore, in the first instance, the missing pieces of the feet and assemble the specimen with a stricter anatomical approach. Proper preservation of fossils in museums is of utmost importance to ensure the integrity and accuracy of palaeontological exhibits. It is also crucial for accurately transmitting scientific knowledge to the community. These

fossils are invaluable evidence of the past, and their proper preservation ensures that researchers and visitors can obtain accurate information about life and historical events on our planet.

Thanks to this restoration effort, visitors will be able to fully appreciate the majesty and history of this ancient dinosaur at the MLP.

The main goal of this paper is to describe a thorough methodology to elaborate a 3D reconstruction of the manus and pes of *Neuquensaurus*. This methodology allows reconstructing the incomplete and poorly preserved skeleton of other sauropod taxa, representing a powerful tool for comparing the biomechanics between different groups of sauropods.

## MATERIAL AND METHODS

**Institutional acronyms.** IANIGLA-PV, Instituto Argentino de Nivología, Glaciología y Ciencias Ambientales, Colección de Paleovertebrados, Mendoza Capital, Mendoza, Argentina;

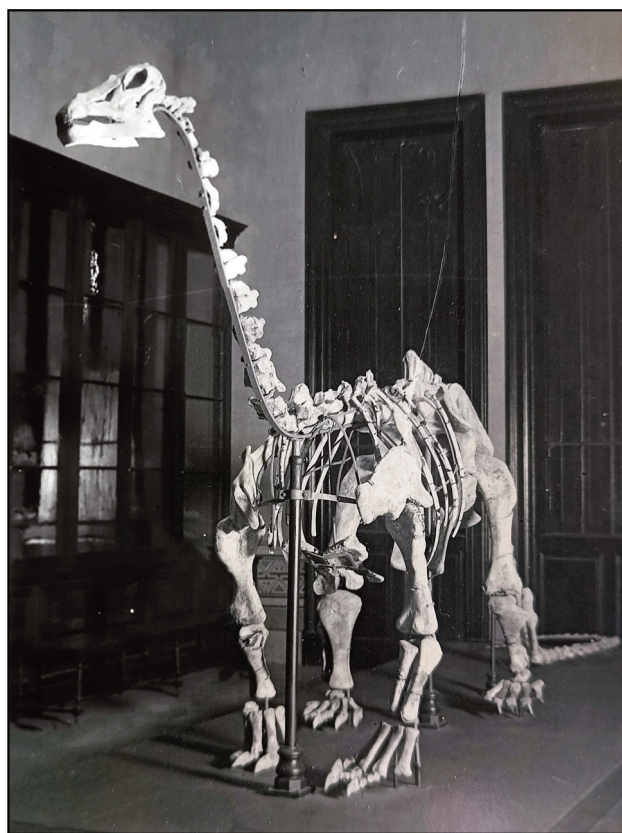


Figure 2. Original montage of *Neuquensaurus australis* specimen from the Museo de La Plata circa early 20th century.

**MLP**, Museo de La Plata, La Plata, Buenos Aires, Argentina; **MLP-CS**, Museo de La Plata, Colección Cinco Saltos, La Plata, Buenos Aires, Argentina; **MPCA**, Museo Provincial 'Carlos Ameghino', Cipolletti, Río Negro, Argentina.

For the reconstruction of the anterior and posterior autopodia of *Neuquensaurus*, elements were used according to the identification of Otero (2010) and Agustín Pérez Moreno (personal observations).

**Metacarpals (MC)**. MLP-CS 1197 (MC II, right), MLP-CS 1189 (MC III, right), MLP-CS 1237 (MC IV, right), and MLP-CS 1238 (MC IV, right). *Argyrosaurus superbus* (Lydekker, 1893; MLP 77-V-29-1) metacarpals were used for metacarpals I and V.

**Astragalus and calcaneus**. A plaster copy of the astragalus (MLP-CS 1216) and a plaster copy of the calcaneus (MLP-CS 1233) were scanned to generate the 3D models.

**Metatarsals (MT)**. MLP-CS 1185 (MT I, right), MLP-CS 1179 (MT I, right), MLP-CS 1180 (MT V, left), MLP-CS 1183 (MT II, left), and MLP-CS 1182 (MT V, left). For metatarsals II, III, and IV, the metatarsals of *Bonitasaura salgadoi* Apesteguía, 2004 (MPCA 460) and *Mendozasaurus neguyelap* González-Riga, 2003 (IANIGLA-PV 077/1-5) were used as references. For both pedals and unguals phalanges, we used as reference the phalanges of *B. salgadoi* (MPCA 460) and *M. neguyelap* (IANIGLA-PV 077/6-12, IANIGLA-PV 078/1-2, IANIGLA-PV 079) and the pedal phalanx MLP-CS 1206 assigned to *Neuquensaurus*.

## RESULTS

### Procedure

In order to reconstruct the autopodia of *Neuquensaurus*, a series of steps (scanning, reconstruction of missing parts, retrodeformation, scaling, texturing, rendering, printing, and mounting; Fig. 3) were carried out for both hand and foot elements. Each of them is detailed below.

**Scanning**. Scanning was carried out with two different scanners, depending on the sample size. We used the NextEngine Ultra HD scanner (<http://www.nextengine.com/>) for metacarpals, astragalus, calcaneus, metatarsals and phalangeal parts of *Neuquensaurus* (MLP-CS 1179, MLP-CS 1180, MLP-CS 1182, MLP-CS 1183, MLP-CS 1185, MLP-CS 1189, MLP-CS 1197, MLP-CS 1206, MLP-CS 1216, MLP-CS 1233, MLP-CS 1237, MLP-CS 1238). With a maximum

resolution of 0.1 mm and a maximum accuracy of 0.125 mm, the NextEngine Ultra HD scanner is an excellent tool for obtaining 3D models of small (3 or 4 cm) to medium (20 or 25 cm) sized parts.

Each part scanned with the NexEngine Ultra HD took about 1–1.5 hours (depending on the hardware). Two scan cycles of 11 turns were performed, obtaining 3D models varying between two and six million points. Cycles take place because when scanning in one axis, information on the antagonist axis is lost; when performing two cycles, the model is completed. The difference between points lies in the total volume of the scanned piece. In this way, excellent quality results were obtained (Fig. 4).

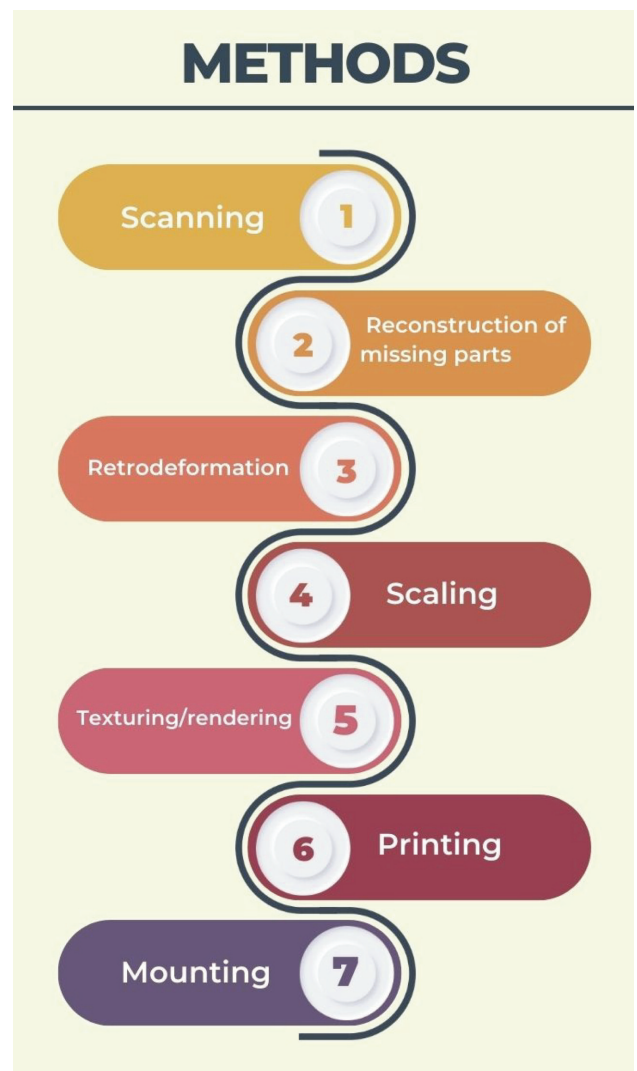


**Figure 3.** Step-by-step flowchart of the methodology developed in this project.

Once the scanning was completed, the post-processing of the model was performed, which included trimming the unwanted surplus, aligning the points, and their subsequent fusion. This step took about five minutes approximately, depending on the model. In this way, excellent mesh quality results were obtained.

On the other hand, the Artec Eva LITE scanner (<https://www.artec3d.com/es/portable-3d-scanners/artec3d>) is more adequate for medium (20 to 25 cm) to large (25 cm to m) sized objects, setting a resolution of 0.2 mm and an accuracy of 0.1 mm. Obtaining 3D models varies between one and three million points. For this reason, we used it to

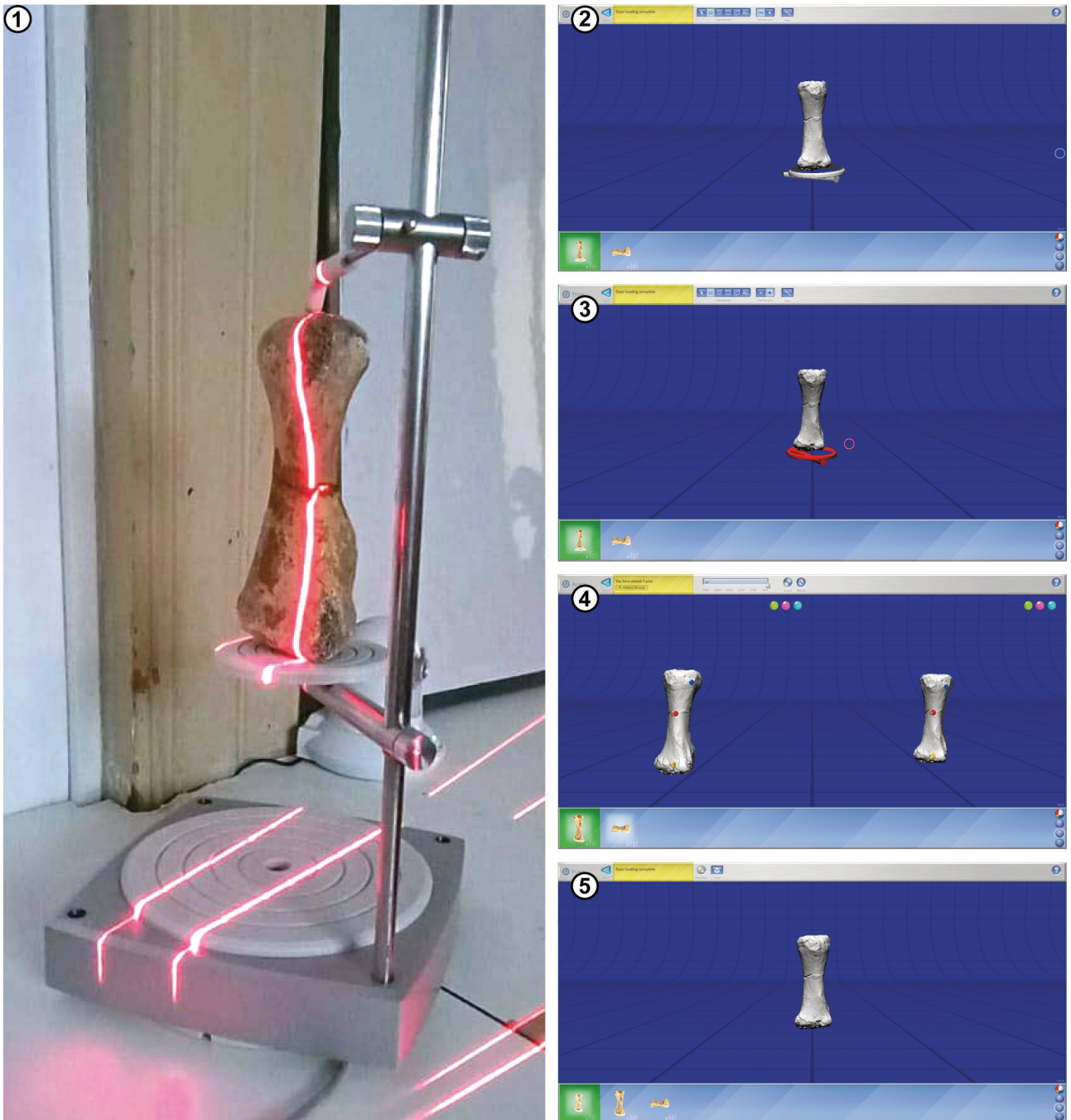
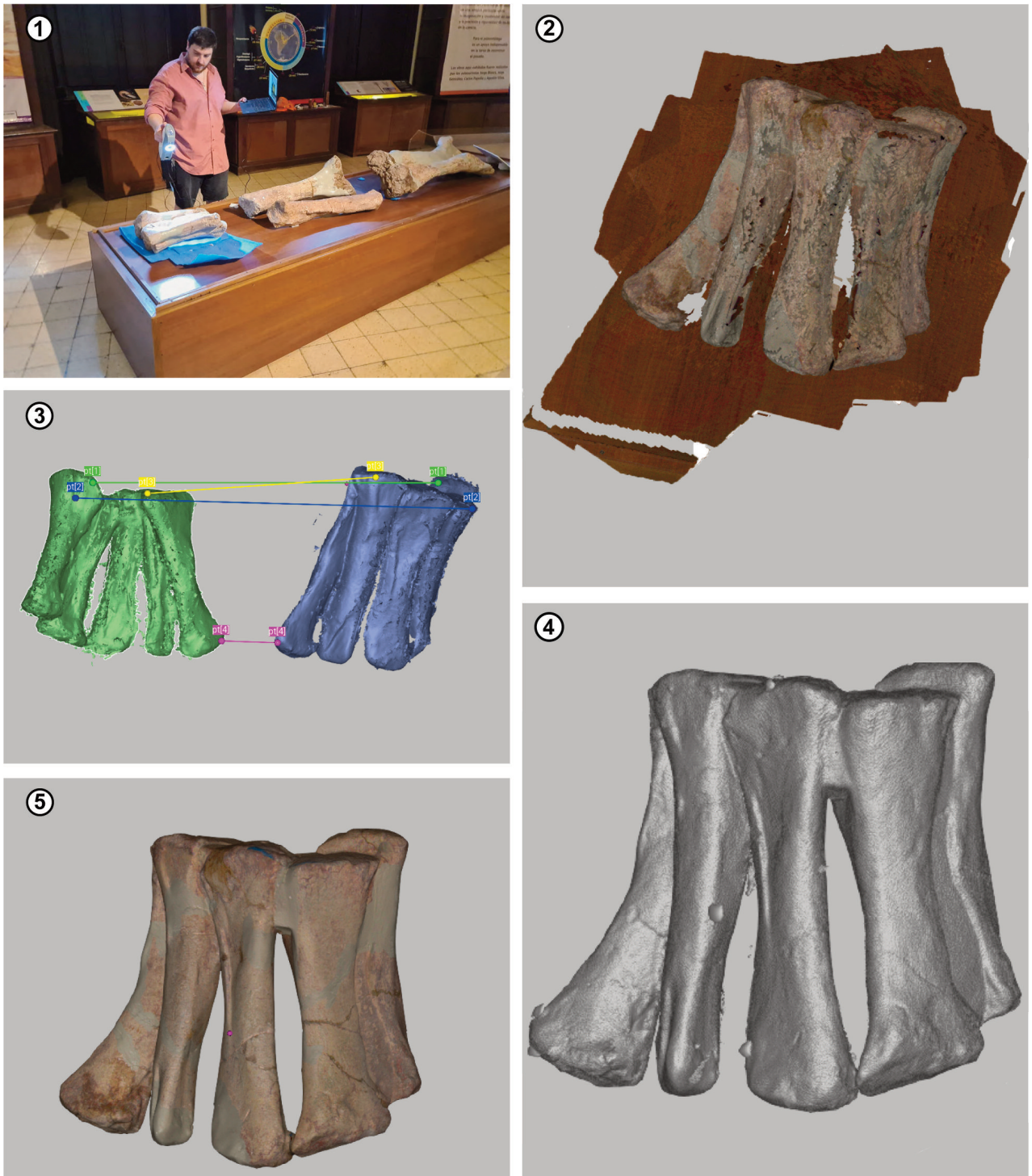


Figure 4. Scanning process with NextEngine Ultra HD of a *Neuquensaurus* metacarpal element; 1, scanning of the element; 2, result of one scanning lap; 3, trimming of the excess information; 4, aligning of the scans by means of dots; 5, final result.

scan the left forelimb of *Argyrosaurus*, which is over 3 m long and exposed in a difficult-to-access place of the museum (Fig. 5). This hand-held scanner provides an excellent solution allowing the fossil to be easily scanned, without

moving the material.

Four scans of the *Argyrosaurus* (humerus, radius, ulna, and metacarpals) were made and processed (High-Definition registration, deletion of excess elements,



**Figure 5.** Scanning process with Artec Eva LITE of the forelimb of *Argyrosaurus*; 1, scanning of the piece; 2, result of a first scan approximation; 3, alignment of the scans with dots; 4, result of the mesh without the texture; 5, final result.

alignment, global registration, fusion, deletion of small objects, mesh simplification, hole closure, and texture application). The 3D imaging took 10 minutes approximately (depending on the size of the bone), and processing took 30 minutes per piece.

It is interesting to note some differences between the two scanning strategies. First, scanning with the Artec Eva LITE takes less time to capture the images but takes longer to post-process the models. In addition, the Artec Eva LITE is a manual type scanner that must be operated all the time by the user at the time of image capture. On the other hand, the NextEngine Ultra HD scanner takes more time to capture the image but less time to post-process it. This is because the NextEngine Ultra HD is a desktop scanner, so it does not require an operator to capture images as it is automatic.

**Retrodeformation.** In general, vertebrate fossils undergo intense taphonomic processes, where plastic deformation or breakage is frequent (Lautenschlager, 2016). When considering biomechanics and range of motion analysis, taphonomic distortion can make articulation of samples difficult or even impossible. The materials assigned to *Neuquensaurus* and the manus of *Argyrosaurus* were damaged and compacted, hence the need to retrodeform these fossils. Regarding the autopodium, it was impossible for it to present symmetry; therefore, the retrodeformation was made manually using Zbrush (Steyer *et al.*, 2010; <https://www.maxon.net/es/zbrush>). The metacarpal elements assigned to *Neuquensaurus* presented the same morphology but belonged to different individuals (Otero, 2010); consequently, these elements exhibited different wear. In order to achieve a more accurate retrodeformation, the best-preserved elements were taken as a basis and their damaged parts were corrected on the basis of the undamaged parts of other overlapping elements (Fig. 6).

**Scaling.** One of the problems to overcome when reconstructing the skeleton of a taxon from other related taxa is the assumption regarding the bones' dimensions. As it was mentioned above, parts of the metacarpal elements of

*Neuquensaurus* were made based on *Argyrosaurus*. The elements of this latter taxon were quadruple the size and much more gracile than the preserved elements of *Neuquensaurus*.

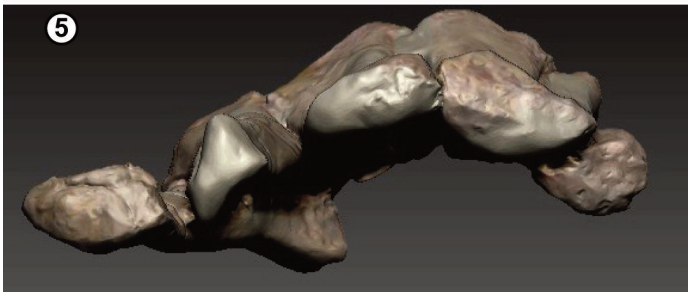
We inferred the size of the metacarpal elements of *Neuquensaurus* based on data collected from a comparative analysis of several related taxa. All titanosaurs with preserved humerus, radius, ulna, and all metacarpal elements (*e.g.*, *Opisthocoelicaudia* Borsuk-Bialynicka, 1977; *Rapetosaurus* Curry Rogers & Forster, 2001; *Dreadnoughtus* Lacovara *et al.*, 2014) were evaluated for the current analysis (Tab. 1). From these taxa, the difference between the length of each metacarpal element with respect to the humerus, radius, and ulna was calculated (Fig. 7; Tab. 1). As a result, we found that titanosaurs have a ratio of 0.3 between the humerus and the metacarpals, and approximately 0.45 between the metacarpals and the zeugopodium elements. Based on the dimensions of the humerus and the zeugopodium bones, the possible measurements of the metacarpal elements with both ratios were calculated. As both calculations did not give the same lengths, we decided to average both to get the closest possible size.

The hind limb elements were processed similarly. The relationship between each metatarsal and the femur, tibia, and fibula was estimated. The same was done to obtain the pedal and ungual phalange measurements. On average, the metatarsals of titanosaurs have a relationship that varies between 0.1 and 0.2 with the femur, and between 0.15 and 0.2 with the zeugopodium. On the other hand, the pedal phalanges have a ratio of 0.45 with the metatarsals, and the ungual phalanges have a ratio that varies between 0.6 and 1 with the metatarsals (see Tab. 2).

**Reconstruction of missing pieces.** To obtain the missing metacarpal elements of *Neuquensaurus* (Fig. 8), we resorted to one of the closest and most complete representative available in the collection of the MLP: *Argyrosaurus* (MLP 77-V-29-1). Once the scan was obtained, the metacarpals were separated from each other and from the sedimentary matrix

---

**Figure 6.** Result of the retrodeformation of the autopodium of *Argyrosaurus* using the Zbrush program before and after retrodeformation; **1**, proximal view without retrodeformation; **2**, retrodeformed proximal view; **3**, frontal view without retrodeformation; **4**, retrodeformed frontal view; **5**, distal view without retrodeformation; **6**, retrodeformed distal view; **7**, posterior view without retrodeformation; **8**, retrodeformed posterior view.



to complete the missing structures. This process was performed with Zbrush.

The metacarpals were separated digitally following their anatomy and texture, separating the remains of sediment

between the bones. In this way, it was possible to visualize for the first time the complete morphology of all the elements individually.

Once all the elements of the *Argyrosaurus* metacarpus

**TABLE 1 – Calculated ratios between anterior stylopodium, zeugopodium, and autopodium elements within Titanosauria.**

|                            | Ratios |       |        |       |      |
|----------------------------|--------|-------|--------|-------|------|
|                            | MC I   | MC II | MC III | MC IV | MC V |
| <i>Opisthocoeliacaudia</i> |        |       |        |       |      |
| Humerus                    | 0.30   | 0.28  | 0.28   | 0.24  | 0.25 |
| Radius                     | 0.47   | 0.45  | 0.44   | 0.38  | 0.39 |
| Ulna                       | 0.38   | 0.36  | 0.35   | 0.30  | 0.31 |
| <i>Argyrosaurus</i>        |        |       |        |       |      |
| Humerus                    | 0.35   | 0.37  | 0.37   | 0.31  | 0.29 |
| Radius                     | 0.56   | 0.60  | 0.59   | 0.49  | 0.46 |
| Ulna                       | 0.50   | 0.53  | 0.52   | 0.44  | 0.41 |
| <i>Rapetosaurus</i>        |        |       |        |       |      |
| Humerus                    | 0.33   | 0.34  | 0.35   | 0.35  | 0.32 |
| Radius                     | 0.47   | 0.48  | 0.50   | 0.50  | 0.46 |
| Ulna                       | 0.47   | 0.48  | 0.49   | 0.49  | 0.45 |
| <i>Mendozasaurus</i>       |        |       |        |       |      |
| Humerus                    | 0.29   | 0.30  | 0.30   | 0.30  | 0.27 |
| Radius                     | 0.46   | 0.46  | 0.46   | 0.48  | 0.43 |
| Ulna                       | 0.45   | 0.45  | 0.45   | 0.46  | 0.42 |
| <i>Epachthosaurus</i>      |        |       |        |       |      |
| Humerus                    | 0.35   | 0.35  | 0.34   | 0.32  | 0.31 |
| Radius                     | 0.58   | 0.57  | 0.56   | 0.52  | 0.51 |
| Ulna                       | 0.53   | 0.52  | 0.51   | 0.47  | 0.46 |
| <i>Malawisaurus</i>        |        |       |        |       |      |
| Humerus                    | 0.35   | 0.33  | 0.28   | 0.21  | 0.00 |
| Radius                     | 0.62   | 0.57  | 0.49   | 0.37  | 0.00 |
| Ulna                       | 0.57   | 0.52  | 0.44   | 0.34  | 0.00 |
| <i>Diamantinasaurus</i>    |        |       |        |       |      |
| Humerus                    | 0.35   | 0.35  | 0.39   | 0.33  | 0.30 |
| Radius                     | 0.55   | 0.56  | 0.61   | 0.52  | 0.48 |
| Ulna                       | 0.53   | 0.54  | 0.59   | 0.50  | 0.46 |

Abbreviations: MC I-V, metacarpals I to V.

TABLE 2 – Calculated ratios between posterior stylopodium, zeugopodium, and autopodium elements within Titanosauria.

|                            | Ratios |       |        |       |      |
|----------------------------|--------|-------|--------|-------|------|
|                            | MT I   | MT II | MT III | MT IV | MT V |
| <i>Opisthocoeliacaudia</i> |        |       |        |       |      |
| Femur                      | 0.11   | 0.13  | 0.14   | 0.13  | 0.10 |
| Tibia                      | 0.19   | 0.22  | 0.25   | 0.22  | 0.17 |
| Fibula                     | 0.18   | 0.22  | 0.24   | 0.22  | 0.17 |
| PhP I                      | 0.43   | -     | -      | -     | -    |
| PhP II                     | -      | 0.5   | -      | -     | -    |
| PhP III                    | -      | -     | 0.4    | -     | -    |
| PhP IV                     | -      | -     | -      | 0.39  | -    |
| PhU I                      | 1      | -     | -      | -     | -    |
| PhU II                     | -      | 0.8   | -      | -     | -    |
| PhU III                    | -      | -     | 0.6    | -     | -    |
| <i>Rapetosaurus</i>        |        |       |        |       |      |
| Femur                      | 0.10   | 0.12  | 0.14   | 0.13  | 0.21 |
| Tibia                      | 0.13   | 0.16  | 0.18   | 0.18  | 0.28 |
| Fibula                     | 0.14   | 0.18  | 0.19   | 0.19  | 0.30 |
| PhP I                      | 0.48   | -     | -      | -     | -    |
| PhP III                    | -      | -     | 0.34   | -     | -    |
| PhU I                      | 1.11   | -     | -      | -     | -    |
| PhU II                     | -      | 0.85  | -      | -     | -    |
| PhU III                    | -      | -     | 0.56   | -     | -    |
| <i>Bonitasaura</i>         |        |       |        |       |      |
| Femur                      | 0.10   | 0.13  | 0.14   | 0.15  | 0.12 |
| Tibia                      | 0.17   | 0.21  | 0.23   | 0.25  | 0.20 |
| Fibula                     | 0.16   | 0.21  | 0.23   | 0.25  | 0.19 |
| PhP III                    | -      | -     | 0.35   | -     | -    |
| PhP IV                     | -      | -     | -      | 0.41  | -    |
| PhU I                      | 0.92   | -     | -      | -     | -    |
| <i>Mendozasaurus</i>       |        |       |        |       |      |
| Femur                      | 0.09   | 0.10  | 0.12   | 0.13  | 0.11 |
| Tibia                      | 0.16   | 0.17  | 0.21   | 0.23  | 0.19 |
| Fibula                     | 0.16   | 0.17  | 0.21   | 0.22  | 0.19 |
| PhP I                      | 0.39   | -     | -      | -     | -    |
| PhP II                     | -      | 0.39  | -      | -     | -    |

TABLE 2 – Continuation

|                       | Ratios |       |        |       |      |
|-----------------------|--------|-------|--------|-------|------|
| PhP III               | -      | -     | 0.28   | -     | -    |
| PhP IV                | -      | -     | -      | 0.4   | -    |
| PhU I                 | 0.95   | -     | -      | -     | -    |
| PhU II                | -      | 0.82  | -      | -     | -    |
| PhU III               | -      | -     | 0.65   | -     | -    |
| <i>Epachthosaurus</i> | MT I   | MT II | MT III | MT IV | MT V |
| Femur                 | 0.14   | 0.16  | 0.18   | 0.19  | 0.16 |
| Tibia                 | 0.19   | 0.23  | 0.26   | 0.27  | 0.23 |
| Fibula                | 0.19   | 0.22  | 0.25   | 0.26  | 0.22 |
| PhP I                 | 0.22   | -     | -      | -     | -    |
| PhP II                | -      | 0.25  | -      | -     | -    |
| PhP III               | -      | -     | 0.22   | -     | -    |
| PhP IV                | -      | -     | -      | 0.20  | -    |
| PhU I                 | 1.12   | -     | -      | -     | -    |
| PhU II                | -      | 1.01  | -      | -     | -    |
| PhU III               | -      | -     | 0.71   | -     | -    |
| <i>Mnyamawamtuka</i>  | MT I   | MT II | MT III | MT IV | MT V |
| Femur                 | 0.12   | 0.14  | 0.17   | 0.16  | 0.11 |
| Tibia                 | 0.20   | 0.23  | 0.27   | 0.26  | 0.17 |
| Fibula                | 0.19   | 0.22  | 0.26   | 0.24  | 0.16 |
| PhP IV                | -      | -     | -      | 0.42  | -    |
| PhU I                 | 0.94   | -     | -      | -     | -    |
| PhU III               | -      | -     | 0.37   | -     | -    |

Abbreviations: **MT I-IV**, metatarsals I to IV; **PhP**, pedal phalanges; **PhU**, ungual phalanges.

were obtained separately, they were anatomically adapted and scaled to complete the *Neuquensaurus* metacarpus. The elements used were metacarpal I and V (Fig. 8.1).

In the case of the hindlimb of *Neuquensaurus*, the reconstruction took a different course. Due to the lack of several elements of the metapodium and acropodium, in this particular case, it was necessary to reconstruct the phalanges I-1 and I-2, the whole of digits II and III, the metatarsal IV and the ungual phalanx of digit IV.

Unlike what happened with the forelimb, the collection of the MLP does not hold close representatives with preserved elements that can be used as replacements for the missing elements in *Neuquensaurus*. For this reason, the missing pieces had to be modeled from scratch. These reconstructions were based on photographs and sketches of other titanosaurs, such as *Mendozasaurus* and *Bonitasaura* (Fig. 8.2).

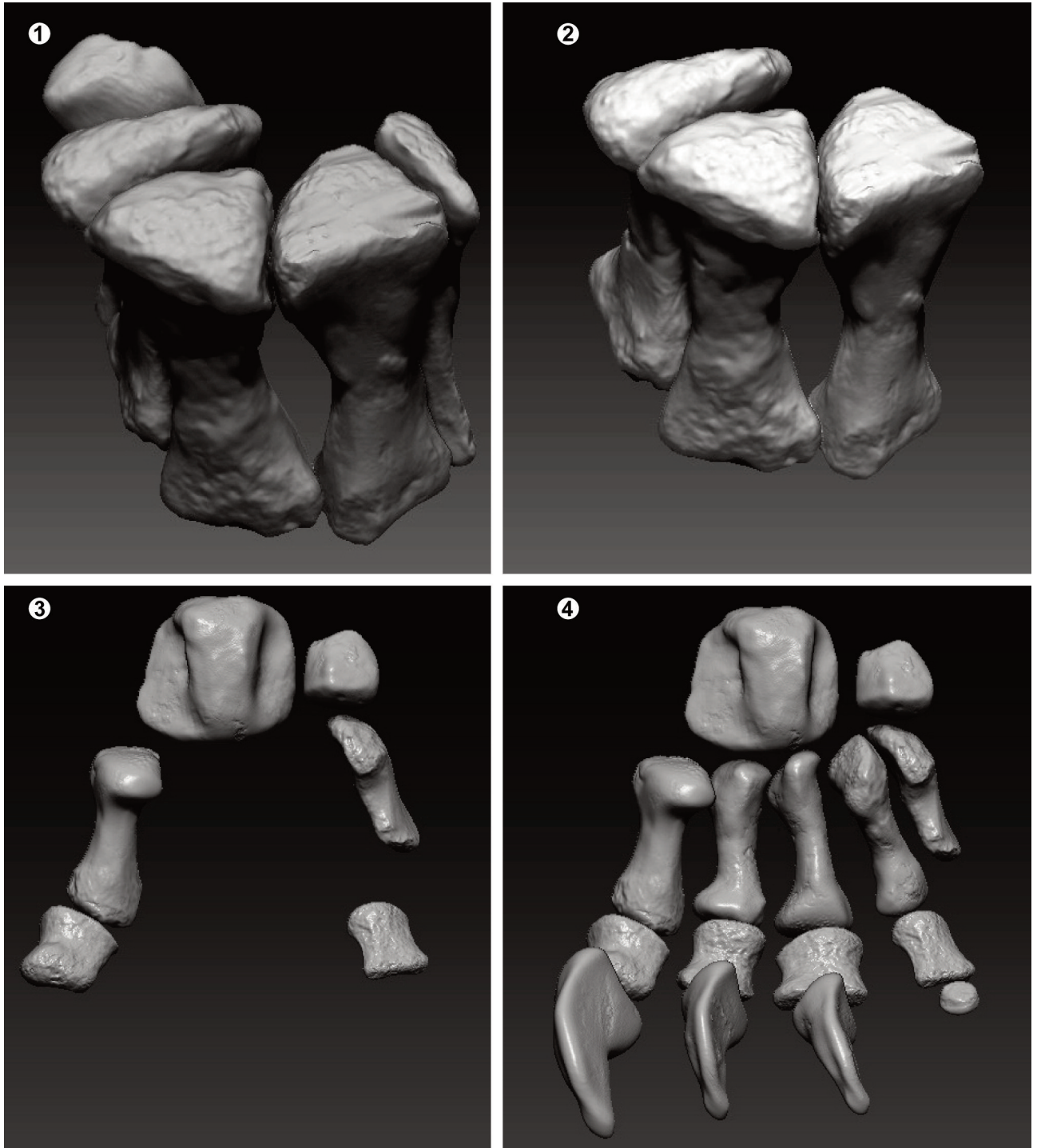
The 3D modeling was done with Zbrush. For this, we used the basic and default tools that come with the



Figure 7. Scaling process; 1, actual size of the *Neuquensaurus* autopodium; 2, size of the autopodium of *Argyrosaurus*; 3, frontal detail view of the reconstructed metacarpals of *Neuquensaurus*; 4, posterior detailed view of the reconstructed metacarpals of *Neuquensaurus*.

software, such as masking brushes, and those for moving, claypolishing, inflating, smoothing, and reducing noise. As for the mesh, we tried to recreate the morphologies, tuberosities, ridges, and valleys, simulating the available

materials. Finally, when the model was finished, a general re-topology (using the tool 'zremesher') was performed to obtain a low number of polygons and make it more manageable and easier to export.



**Figure 8.** Reconstruction of missing parts of *Neuquensaurus*; 1, complete metacarpal elements; 2, reconstructed metacarpal elements; 3, original posterior autopodial elements; 4, complete reconstruction of all elements of the posterior autopodium.

A protocol similar to that used with the metacarpal elements of *Argyrosaurus* was used for the astragalus

and calcaneus of *Neuquensaurus*. The separation and reconstruction of these pieces were carried out since they were fused into a single structure.

**Texturing and rendering.** After completing the 3D modeling process of the fossils, texturing was performed using Substance Painter (<https://www.adobe.com/ar/products/substance3d-painter.html>) software (Fig. 9). During this procedure, textures were applied, and various image channels or maps ('layers') were generated, such as the normal, roughness, and metallic maps, and albedos, among others (Fig. 9.2).

Once the texturing stage was completed, the resulting files were exported to the Marmoset Toolbag 4 (<https://marmoset.co/>) software, where the final rendering was carried out. Thus, the illumination and background of the maps were adjusted, and vignetting was applied to obtain a high-quality image (Fig. 9.3).

Additionally, the 3D model was uploaded to the Sketchfab platform (<https://sketchfab.com/museolp>), where a series of post-production effects were applied to improve its visualization, including color correction, lighting, and model rotation. It is relevant to note that although the model can be visualized in 3D, it is not available for download.

**Printing.** For the 3D printing of the models, a series of technical modeling and scanning processes were carried out to obtain 40 prints. To optimize the details of the bones, both distally and proximally, the designs were cut in the middle of the diaphysis (Fig. 10).

Printing was performed using an Ender 3 V2 printer (Fig. 10.2; Fused Deposition Modeling technology) configured with specific parameters in the Ultimaker Cura 5.2.2 laminator (Fig. 10.1). In particular, a layer height of 0.2 mm, a 10% infill, and a print speed of 50 mm/s were set. The extrusion temperature was also set to 200°C and the hot bed to 50°C. The other parameters were set according to the printer's standard specifications.

As for the material used for printing, we opted for white polylactic acid (PLA) Hellbot filament (refill), which is characterized by its high quality and resistance. This filament allowed obtaining optimal results in terms of precision and detail, which is particularly relevant for printing paleontological elements that require high fidelity in their reproduction (Fig. 10.3).

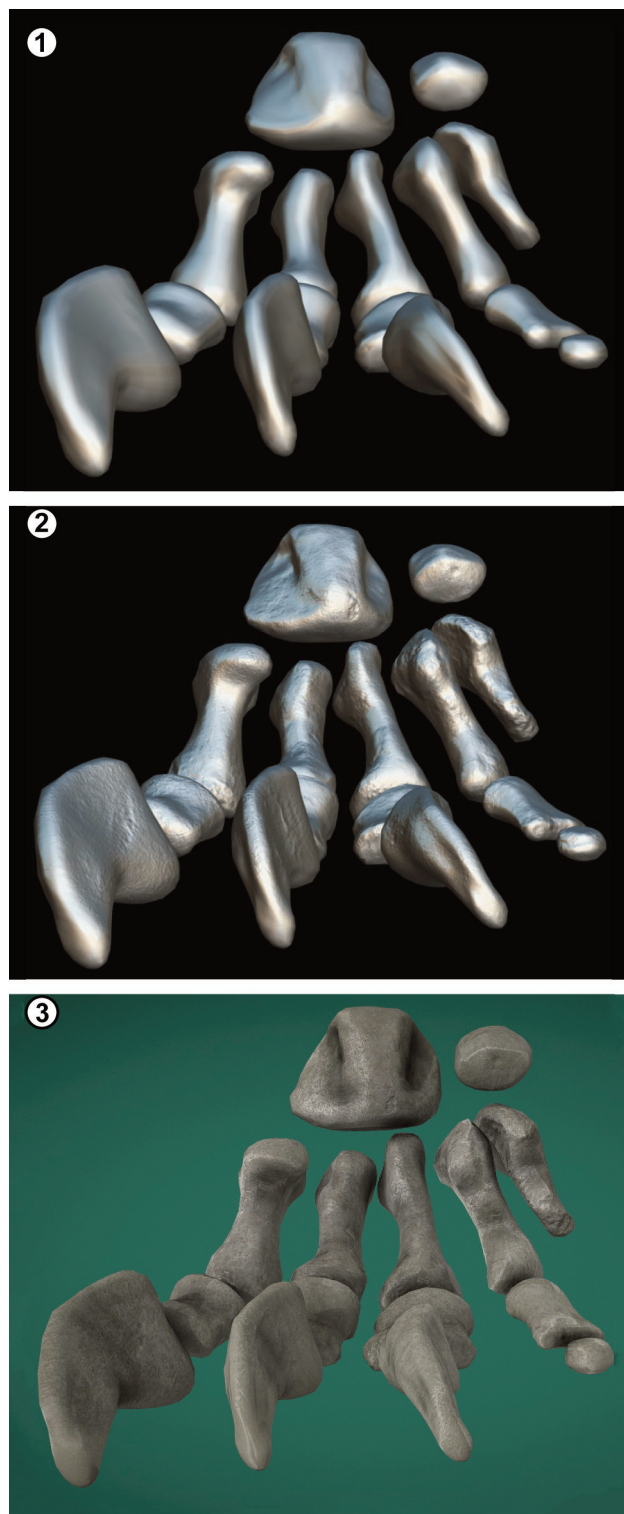


**Figure 9.** Texturing and rendering of the posterior autopodium of *Neuquensaurus*; 1, model without great detail in the mesh and without texture; 2, model with the final mesh; 3, final rendering with texture.

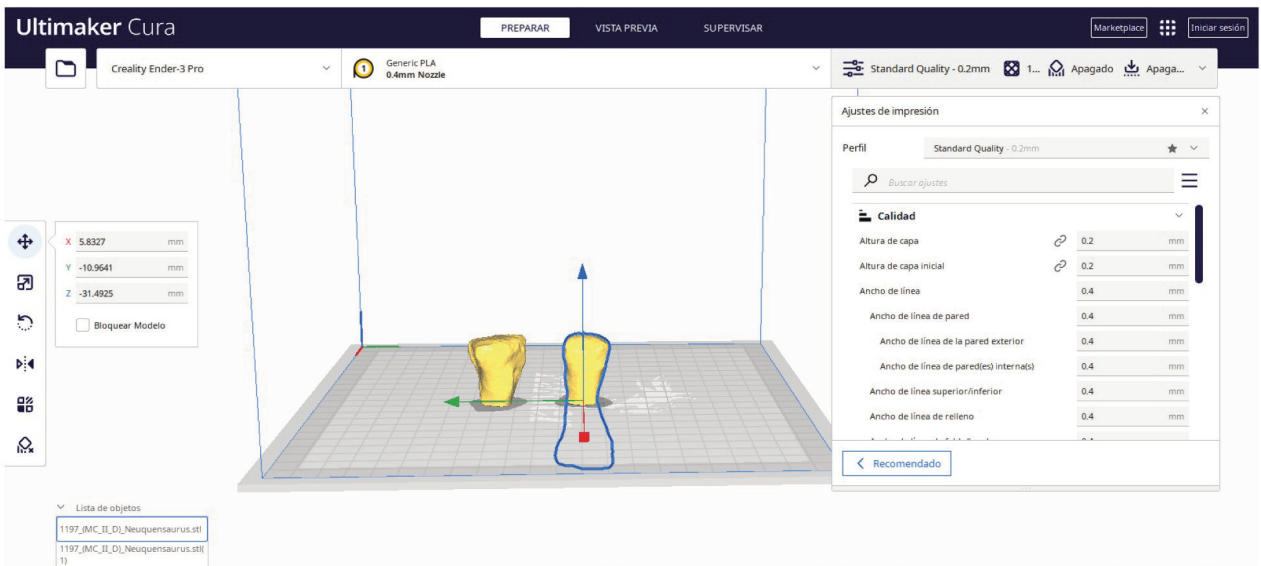
**Painting and mounting.** With the new detailed 3D models of the forelimbs and hindlimbs, the missing elements were accurately reproduced.

One of the final steps in the assembly process was giving a final touch to the 3D printed bones. To achieve a similar appearance to the original fossil bones displayed in the exhibition, the printed replicas were coated with the non-toxic Ecocryl® acrylic resin. This special coating provided durability and protection to the models, ensuring their longevity in the exhibition. Next, technicians meticulously painted the bones with Rust-Oleum® acrylic

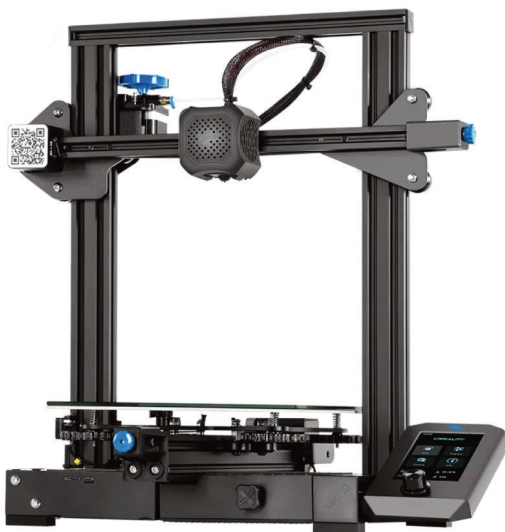
latex painting, paying special attention to details to reproduce the subtle hues and textures of the fossilized remains. The skillful application of paint brought the 3D printed bones to life, which blended seamlessly with the existing skeleton. The result was a stunning and realistic representation of the reconstructed autopodia, perfectly integrated into the already exposed skeleton of *Neuquensaurus*.

Finally, the new elements were mounted. Special attention was paid to anatomical accuracy and alignment, allowing seamless integration with the existing skeleton.

①



②



③



Figure 10. *Neuquensaurus* printing process; 1, working place where the piece to be printed is located; 2, Ender 3 V2 printer with which the printing was made; 3, comparison between the original metatarsal and the printing.

The structure on which skeletal elements were mounted was modified to adapt it to a new and more anatomically correct position by means of new attachments.

## DISCUSSION

### Advantages of 3D techniques

Compared to classical silicone models, 3D techniques offer numerous significant advantages in terms of processing times and costs. Traditional modeling techniques involve a laborious manual process that requires the creation of silicone molds from original fossils (Cunningham *et al.*, 2014). This process can be time-consuming, especially for complex and detailed fossils. In this sense, 3D techniques allow the rapid and accurate capture of 3D models of fossils using specialized scanners.

Furthermore, once the 3D models are captured, processing and preparing the files for printing can also be done more efficiently. Specialized programs and software, such as Zbrush and Substance Painter, allow detailed manipulation and adjustment of the models, making it easier to correct deformations and restore the original shape of the fossils. These processing steps are also performed faster and more efficiently compared to the manual processes required for traditional models.

In terms of cost, 3D techniques also offer a significant advantage. Although acquiring 3D scanners and 3D printing equipment may be an initial investment, in the long term, 3D printing is more cost-effective than creating silicone molds and manufacturing traditional replicas. 3D printing materials, such as FDM (Fused Deposition Modeling) technology, are more affordable than those used in silicone models.

The ability to scale and adjust 3D models digitally provides greater flexibility in terms of cost. Models can be easily modified and resized without creating additional molds, saving additional costs.

### Retrodeformation and its importance in reconstruction

The retrodeformation was carried out using Zbrush. The importance of retrodeformation lies in its ability to accurately represent the morphology and articulation of fossil bones. More precise measurements and calculations

related to the length, angle, and curvature of the bony elements can be made by restoring the original shape of bones and correcting deformations (Otero *et al.*, 2020).

Retrodeformation is a crucial process for restoring the original shape of fossil elements that have suffered deformation or damage during the fossilization process (Boyd & Motani, 2008). In the specific case of the study of *Neuquensaurus*, this technique was used to correct the taphonomic distortion of the autopodial bones. This is especially relevant in the case of *Neuquensaurus*, as it will have implications for the reconstruction of locomotion to the extent that it will allow more precise calculations.

Retrodeformation also allows for better comparison and biomechanical analysis between different specimens and taxa; it provides more reliable data for comparisons between individuals, species, and taxonomic groups, which in turn contributes to a better understanding of the evolution and diversity of animals (Motani, 1997; Zollikofer & de León, 2005; Schlager *et al.*, 2018).

It is important to note that retrodeformation is a complex process that requires experience and knowledge in comparative anatomy and paleontology (Dunlavey, 2008). Each fossil element must be treated individually, taking into account its specific characteristics and state of deformation. In addition, it is essential to base retrodeformation on a solid scientific foundation and the integration of multiple lines of evidence, such as comparative morphology, biomechanics, and paleoecology.

### Applications and implications of 3D printing in paleontology

3D printing technology has revolutionized the way fossils are studied and presented, offering different advantages and new opportunities in research and education, allowing the creation of more affordable replicas (Johnson & Carter, 2019). One of the main applications of 3D printing in paleontology is the creation of exact replicas of fossils. By capturing high-resolution 3D models and 3D printing them, scientists can obtain accurate physical copies of fossil specimens without compromising the original ones (Peterson & Krippner, 2019). This allows detailed study of fossils without restrictions, as researchers can manipulate replicas and make measurements without worrying about

damaging the fragile original bones. Also, models are used for testing and experiments, such as strength testing and biomechanical simulations (Díez Díaz *et al.*, 2020). These physical tools allow researchers to test hypotheses, make accurate measurements and obtain empirical data to support their research (Peterson & Krippner, 2019).

3D printing also facilitates scientific communication and outreach. 3D printed replicas offer a tangible and accessible way to share paleontological findings with the general public, allowing for an interactive and enriching experience (Rahman *et al.*, 2012; Grant *et al.*, 2016). Museums and educational institutions can display printed replicas of fossils in exhibitions, allowing visitors to explore and learn about paleontology in a hands-on and visually engaging way.

In addition, 3D printing has great potential in teaching and learning. 3D printed models allow students to study the anatomy of fossils in a more detailed and understandable way. Depending on the scale and quality of the model, it is possible to examine microscopic details, observe morphological features, and manipulate the models to better understand the structure and function of extinct organisms. This encourages hands-on learning and stimulates interest in paleontology and the natural sciences (Cheng *et al.*, 2020).

## CONCLUSIONS

This contribution provides a comprehensive overview of the reconstruction process for the autopodia of *Neuquensaurus*. The integration of 3D scanning, reconstruction techniques, retrodeformation, scaling, texturing, rendering, 3D printing, and mounting allowed for the accurate restoration and visualization of the fossil elements. The advantages of 3D printing, including cost-effectiveness and accessibility, make it a valuable tool in paleontological research, education, and public outreach. The methodologies presented in this contribution showcase the potential of 3D technologies in advancing our understanding of prehistoric life and making it more accessible to a wider audience.

## ACKNOWLEDGEMENTS

We would like to thank the management of the Museo de La Plata, both Analia Lanteri and Marta Fernández. Also, to the Head of the División Paleontología Vertebrados, Sergio Vizcaíno, as well as to Juan José Moly, Leonel Acosta Burrell, Mauricio Bigurarena Ojeda,

and Bruno Zorzit, who facilitated the work of both the preparation of the materials and their mounting. We also thank Alejandro Otero for his valuable contributions and advice, and Diego Viegas for his advice on 3D models. Finally, we would like to extend our heartfelt gratitude to the reviewers, Martin Hechenleitner and an anonymous reviewer, for their invaluable contributions and insights. This contribution was supported by PIP 11220200102844CO and PICT 2020-2067.

## REFERENCES

- Apesteuguía, S. (2004). *Bonitasaura salgadoi* gen. et sp. nov.: a beaked sauropod from the Late Cretaceous of Patagonia. *Naturwissenschaften*, 91, 493–497.
- Arbour, V. M. & Currie, P. J. (2012). Analyzing taphonomic deformation of ankylosaur skulls using retrodeformation and finite element analysis. *PLoS ONE*, 7(6), 1–13. <https://doi.org/10.1371/journal.pone.0039323>
- Borsuk-Bialynicka, M. (1977). A new camarasaurid sauropod *Opisthoceolicaudia skarzynskii* gen. n., sp. n. from the Upper Cretaceous of Mongolia. *Palaeontologia Polonica*, 37(5), 5–64.
- Boyd, A. A. & Motani, R. (2008). Three-dimensional re-evaluation of the deformation removal technique based on “jigsaw puzzling”. *Palaeontologia Electronica*, 11(2), 7A.
- Breithaupt, B. H., Matthews, N. A., & Noble, T. A. (2003). An integrated approach to three-dimensional data collection at dinosaur tracksites in the Rocky Mountain West. *Ichnos*, 11(1–2), 11–26. <https://doi.org/10.1080/10420940490442296>
- Cheng, L., Antonenko, P. D., Ritzhaupt, A. D., Dawson, K., Miller, D., MacFadden, B. J., Grant, C., Sheppard, T. D., & Ziegler, M. (2020). Exploring the influence of teachers’ beliefs and 3D printing integrated STEM instruction on students’ STEM motivation. *Computers & Education*, 158, 103983. <https://doi.org/10.1016/j.compedu.2020.103983>
- Cunningham, J. A., Rahman, I. A., Lautenschlager, S., Rayfield, E. J., & Donoghue, P. C. J. (2014). A virtual world of paleontology. *Trends in Ecology & Evolution*, 29(6), 347–357. <https://doi.org/10.1016/j.tree.2014.04.004>
- Curry Rogers, K. & Forster, C. A. (2001). The last of the dinosaur titans: a new sauropod from Madagascar. *Nature*, 412(6846), 530–534.
- Cuvier, G. (1796). Notice sur le squelette d’une très grande espèce de quadrupède inconnue jusqu’à présent, trouvé au Paraguay, et déposé au cabinet d’histoire naturelle de Madrid. *Magasin encyclopédique, ou Journal des Sciences, des Lettres et des Arts*, 1, 303–310.
- Díez Díaz, V., Demuth, O., Schwarz, D., & Mallison, H. (2020). The Tail of the Late Jurassic Sauropod *Giraffatitan brancai*: Digital Reconstruction of Its Epaxial and Hypaxial Musculature, and Implications for Tail Biomechanics. *Frontiers in Earth Science*, 8(160). <https://doi.org/10.3389/feart.2020.00160>
- Dunlavey, T. (2008). *Image interpretation is important to paleontology? Case studies in data acquisition, fidelity, and retrodeformation using bilaterally symmetric graptolite (Isograptus and Pseudisograptus) and trilobite (Triarthrus beckii and eatonii) fossils*. [Master Thesis, State University of New York at Buffalo]. Retrieved from <https://www.proquest.com/openview/dc67934b81090978e3f7fe465606b024/1?pq-origsite=gscholar&cbl=18750>
- Gonzalez Riga, B. J. (2003). A new titanosaur (Dinosauria, Sauropoda) from the Upper Cretaceous of Mendoza province, Argentina. *Ameghiniana*, 40(2), 155–172.
- Grant, C. A., MacFadden, B. J., Antonenko, P., & Perez, V. J. (2016).

- 3-D Fossils for k–12 education: A case example using the giant extinct shark *Carcharocles megalodon*. *The Paleontological Society Papers*, 22, 197–209.
- Hatcher, J. B. (1901). *Diplodocus* (Marsh): Its osteology, taxonomy, and probable habits, with a restoration of the skeleton. *Memoirs of the Carnegie Museum*, 1, 1–63.
- Hutchinson, J. R., Anderson, F. C., Blemker, S. S., & Delp, S. L. (2005). Analysis of hindlimb muscle moment arms in *Tyrannosaurus rex* using a three-dimensional musculoskeletal computer model: implications for stance, gait, and speed. *Paleobiology*, 31(4), 676–701. <https://doi.org/10.1666/04044.1>
- Hutchinson, J. R. & Garcia, M. (2002). *Tyrannosaurus* was not a fast runner. *Nature*, 415(1), 1018–1021. [https://doi.org/10.5926/jjep1953.34.1\\_84](https://doi.org/10.5926/jjep1953.34.1_84)
- Janensch, W. (1950). The Vertebral Column of *Brachiosaurus brancai*. *Palaeontographica*, 1(3), 27–93.
- Johnson, E. H. & Carter, A. M. (2019). Defossilization: a review of 3D printing in experimental paleontology. *Frontiers in Ecology and Evolution*, 7, 430. <https://doi.org/10.3389/fevo.2019.00430>
- Klinkhamer, A. J., Wilhite, D. R., White, M. A., & Wroe, S. (2017). Digital dissection and three-dimensional interactive models of limb musculature in the Australian estuarine crocodile (*Crocodylus porosus*). *PLoS ONE*, 12(4), 17–22. <https://doi.org/10.1371/journal.pone.0175079>
- Lacovara, K. J., Lamanna, M. C., Ibric, L. M., Poole, J. C., Schroeter, E. R., Ullmann, P. V., Voegelé, K. K., Boles, Z. M., Carter, A. M., Fowler, E. K., Egerton, V. M., Moyer, A. E., Coughenour, C. L., Schein, J. P., Harris, J. D., Martínez, R. D., & Novas, F. E. (2014). A gigantic, exceptionally complete titanosaurian sauropod dinosaur from southern Patagonia, Argentina. *Scientific Reports*, 4(1), 6196. <https://doi.org/10.1038/srep06196>
- Lautenschlager, S. (2016). Reconstructing the past: Methods and techniques for the digital restoration of fossils. *Royal Society Open Science*, 3(10), 1–18. <https://doi.org/10.1098/rsos.160342>
- Lydekker, R. (1893). The dinosaurs of Patagonia. *Anales Del Museo de La Plata*, 2, 1–14.
- Mallison, H. (2010a). CAD assessment of the posture and range of motion of *Kentrosaurus aethiopicus* Hennig 1915. *Swiss Journal of Geosciences*, 103(2), 211–233. <https://doi.org/10.1007/s00015-010-0024-2>
- Mallison, H. (2010b). The digital *Plateosaurus* I: Body mass, mass distribution and posture assessed using cad and cae on a digitally mounted complete skeleton. *Palaeontologia Electronica*, 13(2), 1–26.
- Mallison, H. (2011). Rearing giants: kinetic-dynamic modeling of sauropod bipedal and tripodal poses. *Biology of the sauropod dinosaurs: Understanding the life of giants* (pp. 237–250). Indiana University Press.
- Mallison, H. & Wings, O. (2014). Photogrammetry in paleontology—a practical guide. *Journal of Paleontological Techniques*, 12(12), 1–31.
- Motani, R. (1997). New technique for retrodeforming tectonically deformed fossils, with an example for ichthyosaurian specimens. *Lethaia*, 30(3), 221–228.
- Otero, A. (2010). The appendicular skeleton of *Neuquensaurus*, a Late Cretaceous saltasaurine sauropod from Patagonia, Argentina. *Acta Paleontologica Polonica*, 55(3), 399–426.
- Otero, A. & Gasparini, Z. (2014). The history of the cast skeleton of *Diplodocus carnegii* Hatcher, 1901, at the Museo de la Plata, Argentina. *Annals of Carnegie Museum*, 82(3), 291–304.
- Otero, A., Moreno, A. P., Falkingham, P. L., Cassini, G., Ruella, A., Militello, M., & Toledo, N. (2020). Three-dimensional image surface acquisition in vertebrate paleontology: a review of principal techniques. *Publicación Electrónica de la Asociación Paleontológica Argentina*, 20(1), 1–14. <http://dx.doi.org/10.5710/PEAPA.04.04.2020.310>
- Paul, G. S. & Chase, T. L. (1989). Reconstructing extinct vertebrates. In E. R. S. Hodges (Ed.), *The Guild Handbook of Scientific Illustration* (pp. 239–256). Van Nostrand Reinhold.
- Peterson, J. E. & Krippner, M. L. (2019). Comparisons of fidelity in the digitization and 3D printing of vertebrate fossils. *Journal of Paleontological Techniques*, 22, 1–9.
- Rahman, I. A., Adcock, K., & Garwood, R. J. (2012). Virtual fossils: a new resource for science communication in paleontology. *Evolution: Education and Outreach*, 5, 635–641.
- Reiss, S. & Mallison, H. (2014). Motion range of the manus of *Plateosaurus engelhardti* von Meyer, 1837. *Palaeontologia Electronica*, 17(1), 1–19.
- Schlager, S., Profico, A., Di Vincenzo, F., & Manzi, G. (2018). Retrodeformation of fossil specimens based on 3D bilateral semi-landmarks: Implementation in the R package “Morpho”. *PLoS ONE*, 13(3), e0194073. <https://doi.org/10.1371/journal.pone.0194073>
- Stevens, K. A. (2013). The articulation of sauropod necks: methodology and mythology. *PLoS ONE*, 8(10), e78572. <https://doi.org/10.1371/journal.pone.0078572>
- Stevens, K. A. & Parrish, J. M. (1999). Neck posture and feeding habits of two Jurassic sauropod dinosaurs. *Science*, 284(5415), 798–800. <https://doi.org/10.1126/science.284.5415.798>
- Steyer, J. S., Boulay, M., & Lorrain, S. (2010). 3D external restorations of stegocephalian skulls using Zbrush: the renaissance of fossil amphibians. *Comptes Rendus Palevol*, 9(6–7), 463–470.
- Sutton, M. D., Rahman, I. A., & Garwood, R. J. (2014). *Techniques for Virtual Palaeontology*. John Wiley & Sons.
- Vidal, D. & Díez Díaz, V. (2017). Reconstructing hypothetical sauropod tails by means of 3D digitization: *Lirainosaurus astibiae* as case study. *Journal of Iberian Geology*, 43(2), 293–305. <https://doi.org/10.1007/s41513-017-0022-6>
- Wedel, M. J. (2003a). The evolution of vertebral pneumaticity in sauropod dinosaurs. *Journal of Vertebrate Paleontology*, 23(2), 344–357.
- Wedel, M. J. (2003b). Vertebral pneumaticity, air sacs, and the physiology of sauropod dinosaurs. *Paleobiology*, 29(2), 243–255. <https://doi.org/10.1017/S0094837300018091>
- Xing, L., Ye, Y., Shu, C., Peng, G., & You, H.-L. (2009). Structure, orientation and finite element analysis of the tail club of *Mamenchisaurus hochuanensis*. *Acta Geologica Sinica*, 83(6), 1031–1040.
- Zollikofer, C. P. E. & de León, M. S. P. (2005). *Virtual Reconstruction. A primer in computer-assisted paleontology and biomedicine*. Wiley.

doi: 10.5710/PEAPA.04.10.2023.483

Recibido: 17 de agosto 2023

Aceptado: 4 de octubre 2023

Publicado: 6 de marzo 2024



This work is licensed under

CC BY-NC 4.0

